SSRG International Journal of Mechanical Engineering
ISSN: 2348-8360/ https://doi.org/10.14445/23488360/IJME-V13I8P110

Volume 13 Issue 8, 113-130, August 2026

Original Article

HAM-Driven Physics-Informed Neural Operator for Stratified Radiative Oldroyd-B/Maxwell Nanofluid Flow with Gyrotactic Bioconvection

D. Vidhya[1], P. Umadevi[2], R. Jeevitha[3], A. Sathya Kala[4], K. Sharmilaa[5]

[1,4]*Department of Mathematics, Dr.N.G.P. Institute of Technology, Coimbatore-641048, Tamil Nadu, India.*
[2]*Department of Mathematics, Dr.N.G.P. Arts and Science College, Coimbatore-641048, Tamil Nadu, India.*
[3]*Department of Mathematics, KGiSL Institute of Technology, Coimbatore -641035, Tamil Nadu, India.*
[5]*Department of Mathematics, PSGR Krishnammal College for Women, Coimbatore-641004, Tamil Nadu, India.*

[1]*Corresponding Author : vidhyad222@gmail.com*

Received: 27 February 2026 Revised: 30 April 2026 Accepted: 24 July 2026 Published: 27 August 2026

Abstract - *For the purpose of simulating stratified radiative Oldroyd-B/Maxwell nanofluid flow induced by gyrotactic microorganisms, this research suggests a new HAM-guided Physics-Informed Neural Operator (HAM-PINO). Nanoparticle concentration diffusion, Rosseland thermal radiation transport, and microorganism conservation laws are coupled with the governing nonlinear viscoelastic momentum equations. The suggested approach incorporates Homotopy Analysis Method convergence-control parameters into operator learning, in contrast to traditional PINNs that are unstable under strong viscoelastic and radiative couplings. This leads to fast convergence across regimes with multiple parameters and stable residual evolution. According to numerical benchmarking, the HAM-PINO solver outperforms the following: RKF45, shooting, DeepONet, FNO, and Transformer-PINO, with a relative L_2-error of 4.2×10^ (-6). The technical results show that as the radiation increases, the heat transfer improves, and the Nusselt number goes up from 1.90 to 2.65. On the other hand, the skin friction goes up from 0.42 to 0.59 due to viscoelastic relaxation. Under stratified stability, the transfer rates of microorganisms also rise. When it comes to bio-nanofluid transport systems that involve multiple physics, HAM-PINO provides a computational operator framework that is both efficient and scalable.*

Keywords – *Physics-Informed Neural Operator, Homotopy Analysis Method, Heat transfer, Nanoparticle concentration diffusion, Oldroyd - B/Maxwell nanofluid flow.*

1. Introduction

Biomedical engineers, polymer processors, and thermal management system developers now use nanofluid transport in viscoelastic settings as a key modelling paradigm [1]. Specifically, non-Newtonian materials such as Oldroyd-B and Maxwell fluids exhibit memory-dependent behaviour due to stress relaxation and retardation, resulting in extremely nonlinear boundary-layer transport [2]. Nanoparticle suspension in such viscoelastic fluids increases thermal conductivity, while associated mass and heat transport adds mathematical stiffness [3]. Radiative heat transfer also takes front stage in hotter settings, where it changes convective stability and greatly increases thermal boundary thickness [4].

The presence of stratification adds another layer of complexity to these systems since it creates temperature and concentration differences across space, leading to flow instabilities caused by buoyancy [5]. Bioconvection dynamics, in which microorganisms swim to produce density gradients that influence fluid motion, is also introduced by gyrotactic bacteria [6]. There are a number of biotech, microbial fuel transport, and bio-inspired cooling technology applications for these types of coupled nanofluid-microorganism interactions [7]. Because of the tight interaction between the viscoelastic stress factors, radiation flow, nanoparticle concentration diffusion, and microbe density evolution, solving the resulting nonlinear PDE system is still a substantial difficulty [8-9].

While Runge-Kutta, gunshot schemes, and spectral collocation are traditional numerical solvers that produce reliable results, they necessitate doing many computations for each parameter regime. The computational cost increases to an unacceptable level when investigating designs with multiple parameters is necessary [10]. With the recent introduction of Physics-Informed Neural Networks (PINNs), which incorporate controlling residuals into the loss function, PDE systems can now train without data. While PINNs work well for moderate systems, they frequently break down when faced with stiff nonlinearities like stratified bioconvection instability, radiative dominance, and Oldroyd-B relaxation coupling [11].

By aiming to approximate the full infinite-dimensional solution operator instead of pointwise functions, neural operator learning presents a fresh paradigm shift [12, 13]. Architectures that are well-suited for quick multiphysics evaluation include DeepONet and Fourier Neural Operators [14]. These models generalise solutions across families of parameters. When residual gradients get stiff under viscoelastic and radiative factors, operator learning still has convergence imbalance [15].

Numerical simulation, physics-informed neural networks, DeepONet designs, and Fourier Neural Operators for multiphysics fluid-flow problems have made progress, but many issues remain. Existing methods focus on viscoelastic nanofluids, radiative transport, or bioconvection phenomena, but stratification, thermal radiation, Oldroyd-B/Maxwell viscoelasticity, nanoparticle diffusion, and gyrotactic microorganism transport are rarely considered together. When solving extremely nonlinear and stiff governing equations, conventional PINN-based frameworks commonly experience training instability, gradient imbalance, and sluggish convergence. Neural operator approaches enhance computing efficiency and parameter generalisation, but residual stiffness and multi-scale interactions degrade their convergence behaviour in tightly coupled viscoelastic-radiative systems. Thus, the literature lacks a robust operator-learning framework that ensures sustained convergence and physical consistency across a vast parameter range.

This paper develops a Homotopy Analysis Method-guided Physics-Informed Neural Operator (HAM-PINO) framework to simulate stratified radiative Oldroyd-B/Maxwell nanofluid flow with gyrotactic bioconvection to overcome these constraints. The main goals are to build a physics-constrained neural operator that can learn solution operators across different physical parameters, to introduce HAM-based convergence-control mechanisms to stabilise residual evolution during training, to study how radiation, viscoelastic relaxation, nanoparticle diffusion, and microorganism transport affect flow behaviour, and to assess the computational accuracy and efficiency.

The HAM-PINO framework differs greatly from previous investigations. Most studies of Oldroyd-B, Maxwell, Jeffrey, Burgers', and Casson nanofluids have used RKF45, shot methods, Keller-box schemes, spectral collocation approaches, and finite-element formulations. Although these methods produce precise results for specific parameter settings, they require repeated computations when physical parameters change. Machine-learning-based methods, including PINNs, DeepONet, Fourier Neural Operators, and Transformer-PINO architectures, have been presented to solve nonlinear partial differential equations. In stiff multiphysics systems with substantial viscoelastic memory effects, thermal radiation, stratification, and microorganism-induced bioconvection, these frameworks often have convergence issues, residual imbalance, and lower accuracy. HAM-PINO incorporates the convergence-control mechanism of the Homotopy Analysis Method directly into neural operator learning, providing stable residual evolution and enhanced parameter generalisation. In addition, this study integrates Oldroyd-B/Maxwell viscoelasticity, radiative heat transfer, nanoparticle concentration transport, stratification effects, and gyrotactic microorganism dynamics into a single operator-learning framework, unlike previous studies. The main originality of the proposed research is this combination, which has not been documented.

The suggested HAM-PINO framework improves on numerical and machine-learning-based techniques. First, it uses the Homotopy Analysis Method's convergence-control capacity and neural operator learning's parameter-generalization strength to resolve convergence instability in PINN- and operator-based solvers. Second, a single computational model includes stratification effects, radiative heat transfer, viscoelastic stress memory, nanoparticle diffusion, and gyrotactic microbe transport. Third, the trained operator makes fast predictions across a wide parameter space, unlike numerical solvers that require repeated simulations for each parameter configuration. These innovations boost highly linked multiphysics system computational efficiency and prediction.

This project aims to create a robust HAM-guided Physics-Informed Neural Operator (HAM-PINO) framework for modelling stratified radiative nanofluid transport and gyrotactic microorganism dynamics. The study aims to formulate a physics-informed neural operator that can learn solution operators across multiple physical parameters, incorporate Homotopy Analysis Method convergence-control mechanisms for residual stabilisation during training, and investigate the effects of radiation, viscoelastic relaxation, nanoparticle concentration diffusion, and microorganism transport on flow characteristics.

Using the Homotopy Analysis Method's convergence deformation in operator learning, this study suggests a HAM-guided Physics-Informed Neural Operator (HAM-PINO) to overcome these shortcomings. In order to stabilise the evolution of residuals during training, HAM introduces a mathematically regulated embedding parameter and a convergence-control factor*. Even when faced with intense radiation, stratification, and microbe coupling, HAM-PINO guarantees smooth convergence, in contrast to traditional PINO frameworks. For complicated stratified Oldroyd-B/Maxwell nanofluid flows, the suggested solver is a new framework that can predict the velocities, temperatures, nanoparticle concentrations, and microbe profiles accurately, quickly, and scalable.

Here remainder of the paper is organized: In Section 2, relevant literature is studied. In Section 3, the technique that has been suggested is laid out in depth. Section 4 delves into the analysis of results. Lastly, Section 5 draws conclusions.

2. Related Works

With the introduction of viscous dissipation and microorganisms, Ishaq et al., [16] examine entropy optimisation in a six-constant Jeffrey fluid through a diverging asymmetric channel. A system of similar ordinary differential equations is systematically used to simplify the analysis of the controlling nonlinear partial differential equations, with the assumptions of lubrication approximations and Debye-Hückel linearisation utilising appropriate dimensionless variables. The homotopy perturbation method, a famous semi-analytic technique, is used to solve the resulting nonlinear Ordinary Differential Equations (ODEs) by transforming them into linear perturbed subproblems. The symbolic solutions for bioconvection, concentration, temperature, and velocity are obtained by solving these subproblems using the DSolve tool in Mathematica. In order to conduct a thorough study, the expressions for these numbers are displayed across several physical parameters. In addition, an ANN model is trained using data taken from these profiles in a Python environment that supports TensorFlow 2.17. A single input layer, two 100-neutrino-neuron hidden layers, and an output layer make up the ANN model. In the hidden layers, the tanh activation function is employed, and the Adam optimiser is used. Many performance indicators are used to assess the accuracy and efficacy of the ANN model. These include validation, relative error, error histograms, regression coefficient (R^2), and Mean Squared Error (MSE). The complex rheology of the six-constant Jeffrey fluid exhibits non-linear patterns, which the ANN predicts with great accuracy. This study's results show that electro-osmotic velocity and magnetic arena within a complex tapering channel considerably affect the non-Newtonian rheology of fluid. Microfluidic system development and targeted medication delivery are two areas of biomedical engineering that stand to benefit greatly from this effort.

The researchers at Alzahrani, H. A., et al., [17] utilised a steady incompressible two-dimensional laminar Glauert wall jet to examine nanoparticle suspension in sodium alginate (NaAlg), a base liquid, under suction and wall slip boundary conditions. Aluminium alloy (AA7075) and Single-Walled Carbon Nanotube (SWCNT) are also taken into account as nanoparticles in a comparative study. The Runge-Kutta-Fehlberg fourth fifth-order (RKF-45) approach and the shooting method are used to numerically solve the reduced Ordinary Differential Equations (ODEs). As the radiation parameter values increase, the results demonstrate that the heat transfer performance of NaAlg−SWCNT Casson nanofluid is better than that of NaAlg−AA7075 Casson nanoliquid. The heat transfer rate of both nanoliquids decreases when the Casson parameter increases, whereas the opposite tendency is observed with improved radiation parameter values.

The dynamics flow of magnetohydrodynamic Burgers' fluid caused by a stretched cylinder are studied by Mebarek-Oudina et al., [18], with a focus on the consequences of internal heat generation and absorption. The system's thermal energy transfer properties are investigated by incorporating a heat source that is dependent on temperature. To use boundary layer theory to simplify the controlling PDEs into a typical system of ordinary differential equations by applying similarity transformations. To get the right answers for the velocity and temperature profiles, the BVP4C approach is used. The impact of different physical parameters on thermal and flow profiles is shown graphically with thorough analytical interpretations to back it up. A review of the relevant literature confirms the reliability and importance of our findings, lending credence to our methodology. Advancements in biomedical device development may benefit from this research's useful insights into the fluid and thermal behaviours of Burgers' fluids.

With a particular emphasis on potential uses in geothermal and renewable energy research, Ketchate et al., [19] investigate how heat radiation and magnetic fields affect the beginning of a layer saturated by a Voigt fluid. Complex fluids with non-Newtonian rheology owing to polymers, suspended particles, or bio-geochemical interaction are used in many geothermal reservoirs, subsurface heat storage units, and exchangers. To optimise heat extraction, improve long-term reservoir presentation, and prevent undesirable thermal stratification, it is vital to understand the stability of thermally driven flow in such situations. In order to find the critical Reynolds number, which depends on Hartmann, Darcy, radiative, Richardson, and Prandtl numbers, a linear stability study is carried out. The results demonstrate that the effective permeability to porous matrix, viscous dissipation, then flow stabilisation is all improved with an increase in the Darcy number, which in turn raises the critical instability threshold. Similarly, a Lorentz damping force that suppresses transverse disturbances is produced by a larger magnetic field, which is represented by the Hartmann number, and this force plays a significant role in stabilising MHD. By reducing temperature gradients and improving effective thermal diffusion, the radiation parameter helps stabilise flows as well. Also, the viscoelastic parameter in the Kelvin-Voigt theory introduces a memory-driven elastic resistance which absorbs shocks and greatly postpones instability onset. At low wavenumbers, the Prandtl number has a dual effect that depends on the Reynolds number; however, in high wavenumber regimes, it has an exclusively stabilising influence, and it is crucial in controlling thermal diffusion, shear, then viscoelasticity. Richardson number, which quantifies buoyancy-shear competition, has the opposite impact and destabilises the system: increased buoyancy forces amplify natural convection motions, which in turn makes the system more perturbation sensitive and speeds up the instability transition.

To discover quantitatively that the stability threshold is raised by 25% for an increase in Hartmann number and modified by 10% for changes in viscoelastic coefficient. Radiation from heat sources raises the cutoff by 12%. Raising the Richardson number often lowers the critical threshold by 20% to 30%, depending on the wavenumber domain, but it drops by about 25% overall.

This research sheds light on how to optimise and design geothermal then renewable energy schemes by controlling hydrodynamic and thermal stability, which is crucial for better efficiency, better heat transfer, then safe operation over the long term. Heat then mass transfer in a Magnetohydrodynamic (MHD) Casson Fluid (CF) flow over an exponentially porous stretched sheet is discussed in the article by Radhika and Dharmendar Reddy [20]. Various factors are considered in the analysis, including chemical reactions, viscous dissipation, thermal radiation, velocity, and thermal slips. The features of Casson fluid are differentiated from Newtonian fluids by considering a well-known Casson model. The geometry that is being considered is used to model the present physical issue.

In order to simplify the set of connected nonlinear PDEs into a set of nonlinear ODEs, the corresponding similarity conversions are used. To solve these simplified non-dimensional controlling flow field equations numerically, the Keller-Box method is used. The physical behaviour of different control parameters is illustrated via tables and pictures. This study found that increasing the value of the CF parameter improved the temperature profile and decreased the velocity profile. When the velocity slip factor was raised, the velocity field shrank, and the temperature and concentration contours shrank as well. A decrease in profile was seen when the chemical reaction component concentration increased. Identical results described in this study do, in fact, show a striking agreement with answers that have been published in the scholarly literature before. The goal of this research is to enhance our sympathetic of fluid flow in various engineering and environmental contexts where it is prevalent, such as in the chemical processing industries, environmental control technologies, geothermal energy extraction, and thermal management.

Critical literature review shows that most studies use classical numerical approaches for viscoelastic nanofluid flow or machine-learning frameworks to solve individual differential equation classes. Operator-learning frameworks that address viscoelastic stress memory, heat radiation, nanoparticle diffusion, stratification effects, and microorganism-induced bioconvection have received little attention. Additionally, neural operator models rarely have convergence-control mechanisms for stabilising training under tightly coupled nonlinear situations. These findings inspired the HAM-guided Physics-Informed Neural Operator framework.

Table 1. Comparison of existing studies and proposed HAM-PINO framework

Study	Numerical / AI Method	Radiation	Viscoelasticity	Bioconvection	Neural Operator	Convergence Control
Ishaq et al., [16]	HPM + ANN	No	Jeffrey	Yes	No	No
Alzahrani et al., [17]	RKF45 + Shooting	Yes	Casson	No	No	No
Mebarek-Oudina et al., [18]	BVP4C	No	Burgers	No	No	No
Ketchate et al., [19]	Stability Analysis	Yes	Kelvin-Voigt	No	No	No
Radhika and Reddy [20]	Keller-Box	Yes	Casson	No	No	No
PINN-Based Models	PINN	Partial	Partial	No	No	No
DeepONet	Neural Operator	Partial	Partial	No	Yes	No
FNO	Neural Operator	Partial	Partial	No	Yes	No
Proposed HAM-PINO	HAM + PINO	Yes	Yes	Yes	Yes	Yes

Table 1 compares representative research and modern operator-learning frameworks. The majority of numerical studies focus on non-Newtonian fluid models and transport mechanisms. Modern neural-operator topologies improve computational efficiency but lack convergence-control techniques for stiff multiphysics systems. The novel HAM-PINO framework accounts for viscoelastic relaxation, radiative transport, nanoparticle diffusion, stratification, and gyrotactic bioconvection while combining operator learning with HAM-based convergence stabilisation. The proposed method differs other prior methods in its greater physical coverage and improved convergence.

3. Proposed Framework: HAM-Guided Physics-Informed Neural Operator for Stratified Radiative Oldroyd-B/Maxwell Nanofluid with Gyrotactic Microorganisms

This section presents a technically advanced and mathematically enriched framework entitled and Figure 1 explains the workflow of proposed model:

Figure 1 Detailed workflow of the proposed HAM-PINO framework illustrating parameter initialization, governing equation formulation, similarity transformation, HAM-based convergence-control integration, neural operator training, residual evaluation, adaptive weight updating, validation, and engineering output prediction.

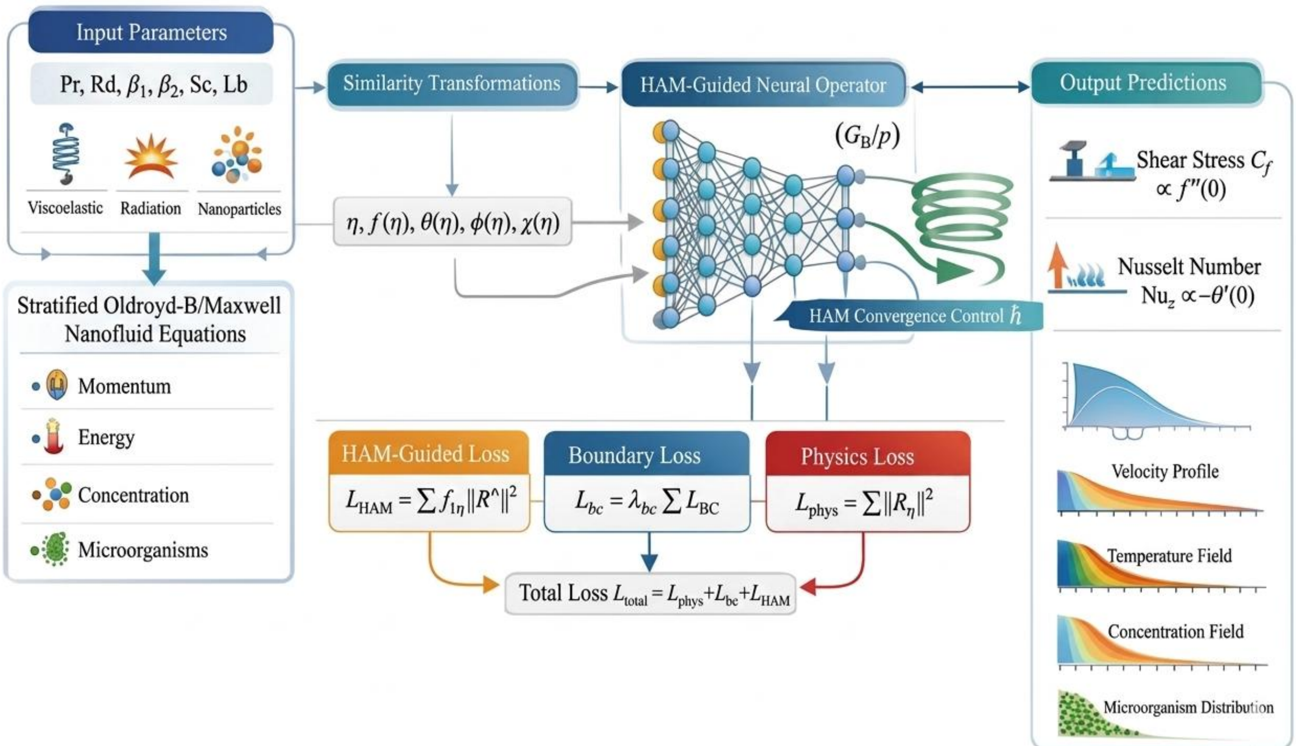

Fig. 1 Physics-informed neural operator flow diagram

HAM-Guided Physics-Informed Neural Operator (HAM-PINO) for modeling stratified boundary-layer flow of Oldroyd-B and Maxwell nanofluids, incorporating thermal radiation, double stratification, and gyrotactic microorganism transport. The novelty of the proposed methodology lies in integrating:

Physics-Informed Neural Operators (PINO) for infinite-dimensional solution learning.

Oldroyd-B/Maxwell viscoelastic constitutive physics.

Homotopy Analysis Method (HAM) guided residual stabilization.

Radiative nanofluid energy transport with microorganism bioconvection coupling.

Unlike classical PINNs that solve at discrete points, the proposed operator framework learns the entire nonlinear solution mapping, while HAM constructs a mathematically consistent convergence-guided training path.

Physical Configuration and Stratified Bioconvective Nanofluid Model.

The considered system involves a two-dimensional steady stratified nanofluid flow over a stretching sheet.

The fluid is viscoelastic, obeying either the Maxwell model (single relaxation time) or the Oldroyd-B model (relaxation + retardation).

In addition, the flow contains: nanoparticles (thermal enhancement), thermal radiation (high-temperature effects) and gyrotactic microorganisms (bioconvection).

The velocity field is:

$$V=(u(x,y), v(x,y)) \tag{1}$$

The flow is incompressible, hence:

$$\frac{\partial u}{\partial x} + \frac{\partial v}{\partial y} = 0 \tag{2}$$

The stratification introduces spatial variation in temperature and concentration, causing buoyancy gradients.

Thus, the framework is essential because classical CFD becomes unstable under:

Viscoelastic nonlinear stress coupling.

Microorganism-induced density instability.

Radiative heat flux dominance.

Stratified mixed convection feedback. This motivates a data-efficient operator-learning physics solver.

3.1. Governing Equations for Oldroyd-B/Maxwell Stratified Nanofluid Flow

Momentum Equation with Viscoelastic Stress.

For an Oldroyd-B fluid, the constitutive stress relation introduces two timescales: relaxation time λ_1 Then the retardation time λ_2.

The nonlinear momentum equation becomes:

$$u\frac{\partial u}{\partial x} + v\frac{\partial u}{\partial y} = v\frac{\partial^2 u}{\partial y^2} + \lambda_1\left(u^2\frac{\partial^2 u}{\partial x^2}\right) - \lambda_2\left(v\frac{\partial^3 u}{\partial y^3}\right) \tag{3}$$

For Maxwell fluid, $\lambda_2 = 0$

Why this matters: viscoelastic stresses store deformation memory, making the PDE strongly nonlinear and stiff.

3.1.1. Energy Equation with Radiation and Nanofluid Transport

The thermal balance under Rosseland approximation is:

$$u\frac{\partial T}{\partial x} + v\frac{\partial T}{\partial y} = \alpha\frac{\partial^2 T}{\partial y^2} - \frac{1}{\rho c_p}\frac{\partial q_r}{\partial y} \tag{4}$$

Radiative heat flux:

$$q_r = -\frac{4\sigma^*}{3k^*}\frac{\partial T^4}{\partial y} \tag{5}$$

Linearization yields:

$$T^4 \approx 4T_\infty^3 T - 3T_\infty^4 \tag{6}$$

Thus:

$$\frac{\partial q_r}{\partial y} = -\frac{16\sigma^* T_\infty^3}{3k^*}\frac{\partial^2 T}{\partial y^2} \tag{7}$$

3.1.2. Nanoparticle Concentration Equation

Including Brownian diffusion and stratification:

$$u\frac{\partial C}{\partial x} + v\frac{\partial C}{\partial y} = D_B\frac{\partial^2 C}{\partial y^2} \tag{8}$$

3.1.3. Gyrotactic Microorganism Conservation

Microorganisms produce bioconvective instability:

$$u\frac{\partial N}{\partial x} + v\frac{\partial N}{\partial y} = D_m\frac{\partial^2 N}{\partial y^2} \tag{9}$$

3.2. Similarity Transformations and Dimensionless Stratified System

To reduce complexity while preserving stratification physics:

$$\eta = y\sqrt{\frac{a}{\nu}} \tag{10}$$

Stream function:

$$\psi = \sqrt{a\nu}\, x f(\eta) \tag{11}$$

Velocity components:

$$u = axf'(\eta), v = -\sqrt{a\nu} f(\eta) \tag{12}$$

Dimensionless temperature, concentration, microorganism density:

$$\theta(\eta) = \frac{T - T_\infty}{T_w - T_\infty}, \phi(\eta) = \frac{C - C_\infty}{C_w - C_\infty}, \chi(\eta) = \frac{N - N_\infty}{N_w - N_\infty} \tag{13}$$

3.2.1. Reduced Nonlinear ODE System

Momentum:

$$f''' + ff'' - (f')^2 + \beta_1 ff^{(4)} - \beta_2 f'' f''' = 0 \tag{14}$$

Energy:

$$\theta'' + Prf\theta' + Rd\,\theta'' = 0 \tag{15}$$

Nanoparticle:

$$\phi'' + Scf\phi' = 0 \tag{16}$$

Microorganisms:

$$\chi'' + Lbf\chi' = 0 \tag{17}$$

Each parameter explains real physics:

Pr: momentum vs thermal diffusivity, Rd: radiation dominance, β_1, β_2: Oldroyd-B viscoelastic memory, Sc: mass diffusion balance and Lb: bioconvection Lewis number

3.3. Physics-Informed Neural Operator Architecture

Unlike PINNs approximating $f(\eta)$ pointwise, Neural Operators learn:

$$\mathcal{G}: \mathcal{F}(p) \to u(\eta) \tag{18}$$

where p denotes parameter space:

$$p = (Pr, Rd, \beta_1, \beta_2, Sc, Lb) \tag{19}$$

Thus, the operator outputs full field solutions instantly for unseen regimes.

Operator network:

$$u(\eta) = \mathcal{G}_\Theta(p)(\eta) \tag{20}$$

This is novel because stratified Oldroyd-B bioconvection is rarely solved with operator learning.

3.4. HAM-Guided Residual Evolution Strategy

Standard PINO training suffers from stiff residual imbalance. HAM and PINO are integrated via residual-guided convergence-control.

In the proposed framework, the neural operator learns the nonlinear solution operator that maps physical parameters to flow, temperature, concentration, and microbe fields.

The Homotopy Analysis Method also controls residual error evolution during training with convergence-control parameters. Each optimisation iteration evaluates and weights the governing PDE residuals using the HAM deformation approach.

Stiff viscoelastic-radiative interactions cause instability, but this adaptive weighting method reduces gradient imbalance. Thus, the neural operator learns the solution manifold, and the HAM component leads convergence toward physically consistent solutions.

Therefore, the Homotopy Analysis Method constructs a convergence deformation:

$$u(\eta; q) = u_0(\eta) + q \sum_{m=1}^{\infty} u_m(\eta) \tag{21}$$

Embedding parameter $q \in [0,1]$smoothly transitions:

- $q = 0$: initial guess
- $q = 1$: full solution

HAM introduces convergence controller $\hbar$:

$$\mathcal{L}[u_m - \chi_m u_{m-1}] = \hbar R_{m-1} \tag{22}$$

This guides neural residual minimization, improving stability. Hence, training is not blind minimization but mathematically steered deformation.

3.5. Loss Formulation with HAM-Weighted Physics Constraints

The residual vector:

$$\mathrm{R} = \left(R_f, R_\theta, R_\phi, R_\chi\right) \tag{23}$$

Physics-informed loss:

$$\mathcal{L}_{phys} = \sum_{i=1}^{4} \| R_i \|^2 \tag{24}$$

HAM adaptive weighting:

$$\mathcal{L}_{HAM} = \sum_{m=1}^{M} \hbar_m \| R^{(m)} \|^2 \tag{25}$$

Boundary loss:

$$\mathcal{L}_{bc} = | f(0) |^2 + | f'(0) - 1 |^2 + | \theta(0) - 1 |^2 + | \phi(0) - 1 |^2 + | \chi(0) + 1 |^2 \tag{26}$$

Total training objective:

$$\mathcal{L}_{total} = \mathcal{L}_{phys} + \lambda_{bc}\mathcal{L}_{bc} + \lambda_{HAM}\mathcal{L}_{HAM} \tag{27}$$

3.6. Algorithmic Workflow of HAM-PINO Solver

The overall computational pipeline: Define parameter sampling space, Initialize HAM deformation guess, Train Neural Operator on PDE residual, Update $\hbar$-weights using residual slope and iterate until operator convergence.

Stopping criterion:

$$\| \mathrm{R} \| < 10^{-6} \tag{28}$$

Novelty: This creates a convergence-monitored neural operator, absent in existing viscoelastic nanofluid literature.

3.7. Output Metrics and Physical Quantities of Interest

The trained framework provides direct evaluation of:

Skin friction coefficient:

$$C_f \propto f''(0) \tag{29}$$

Local Nusselt number:

$$Nu_x \propto -\theta'(0) \tag{30}$$

These quantify shear stress and radiative heat transfer enhancement in stratified Oldroyd-B/Maxwell bioconvection.

Algorithm 1 HAM-Guided Physics-Informed Neural Operator (HAM-PINO) Solver

Input: Physical parameters: $Pr, Rd, Sc, Lb, \beta_1, \beta_2$, Domain: $\eta \in [0, \eta_{\max}]$

Governing nonlinear operators: Momentum: R_f Energy: R_θ Concentration: R_ϕ .Microorganisms: R_χ.

Boundary conditions at $\eta=0$: $f(0)=0, f'(0)=1, \theta(0)=1, \phi(0)=1, \chi(0)=1$

Far-field conditions as $\eta \to \infty$: $f'(\infty) \to 0, \theta(\infty) \to 0, \phi(\infty) \to 0, \chi(\infty) \to 0$

HAM convergence-control parameters: $\hbar_m$, $m=1,\ldots,M$ and Neural operator network parameters: Θ

Output: Solution fields: $f(\eta), \theta(\eta), \phi(\eta), \chi(\eta)$ then Engineering metrics: $C_f \propto f''(0), Nu_x \propto -\theta'(0)$.

Step 1: Parameter Sampling Initialization

1. Generate training samples in parameter space:

$$p^{(k)} = \{Pr, Rd, Sc, Lb, \beta_1, \beta_2\}_{k=1}^{N_p}$$

2. Generate collocation points:

$$\eta_j \sim U(0, \eta_{\max})$$

Step 2: Construct Similarity-Based PDE Residual Operators

Define residual functions:

- Momentum residual:

$$R_f = f''' + ff'' - (f')^2 + \beta_1 ff^{(4)} - \beta_2 f'' f'''$$

- Energy residual:

$$R_\theta = (1+Rd)\theta'' + Prf\theta'$$

- Concentration residual:

$$R_\phi = \phi'' + Scf\phi'$$

- Microorganism residual:

$$R_\chi = \chi'' + Lbf\chi'$$

Step 3: Initialize Neural Operator Architecture

3. Define Physics-Informed Neural Operator:

$$G_\Theta(p)(\eta) \to \{f, \theta, \phi, \chi\}$$

4. Initialize weights Θrandomly.

Step 4: HAM-Based Deformation Initialization

5. Construct HAM deformation series:

$$u(\eta; q) = u_0(\eta) + q \sum_{m=1}^{M} u_m(\eta)$$

Where $q \in [0,1]$: embedding parameter, u_m: HAM correction term and u_0: initial guess

6. Assign convergence-control parameters:

$$\hbar_m \in (-1, 0)$$

Step 5: Define Hybrid HAM-PINO Loss Function

7. Compute physics residual loss:

$$L_{phys} = \|R_f\|^2 + \|R_\theta\|^2 + \|R_\phi\|^2 + \|R_\chi\|^2$$

8. Compute boundary condition loss:

$$L_{bc} = |f(0)|^2 + |f'(0)-1|^2 + |\theta(0)-1|^2 + |\phi(0)-1|^2 + |\chi(0)-1|^2$$

9. HAM-guided residual weighting:

$$L_{HAM} = \sum_{m=1}^{M} \hbar_m \|R^{(m)}\|^2$$

10. Total loss function:

$$L_{total}=L_{phys}+\lambda_{bc}L_{bc}+\lambda_{HAM}L_{HAM}$$

Step 6: Training via HAM-Stabilized Optimization Loop
Repeat until convergence:

11. Forward evaluation:
$$\{f,\theta,\phi,\chi\}=G_{\Theta}(p)(\eta)$$
12. Compute PDE residuals:
$$R_f,R_{\theta},R_{\phi},R_{\chi}$$
13. Evaluate total loss:
$$L_{total}$$
14. Update neural parameters using Adam optimizer:
$$\Theta\leftarrow\Theta-\alpha\nabla_{\Theta}L_{total}$$
15. HAM residual slope adaptation:
$$\hbar_m^{new}=\hbar_m^{old}-\gamma\frac{\partial\|R^{(m)}\|}{\partial m}$$
16. Check stopping criterion:
$$\|R\|<10^{-6}$$

Step 7: Post-Processing and Engineering Output Evaluation

17. Compute skin friction coefficient:
$$C_f=f''(0)$$
18. Compute local Nusselt number:
$$Nu_x=-\theta'(0)$$
19. Compute nanoparticle mass transfer:
$$Sh_x=-\phi'(0)$$
20. Compute microorganism density flux:
$$Nm_x=-\chi'(0)$$

Step 8: Return Full Operator Solution Family

21. Output complete predicted profiles:
$$f(\eta),\theta(\eta),\phi(\eta),\chi(\eta)$$

for arbitrary unseen parameter sets:
$$p^*=(Pr^*,Rd^*,Sc^*,Lb^*,\beta_1^*,\beta_2^*)$$

4. Results and Discussion

Table 2. Physical parameters and dimensionless numbers used in the HAM-PINO framework

Symbol	Parameter Name	Physical Meaning	Typical Range in Study
Pr	Prandtl Number	The ratio of heat diffusivity to momentum diffusivity	0.7 - 10
Rd	Radiation Parameter	Strength of thermal radiation heat flux contribution	0 - 5
β_1	Oldroyd-B Relaxation Parameter	Elastic memory effect due to fluid relaxation time	0 - 1
β_2	Oldroyd-B Retardation Parameter	Stress retardation influence on momentum diffusion	0 - 1
Sc	Schmidt Number	The ratio of mass diffusivity to momentum diffusivity	0.5 - 5
Lb	Bioconvection Lewis Number	Ratio of the diffusivity of microorganisms to the diffusivity of heat	1 - 10

The governing dimensionless parameters' ranges were chosen using viscoelastic nanofluid transport, radiative heat transfer, and bioconvection investigations. The radiation parameter range (0-5) indicates moderate to strong radiative transport, while the Prandtl number range (0.7-10) depicts fluids with different thermal diffusivities. To study viscoelastic memory effects, relaxation and retardation parameters were varied between 0 and 1.

The Schmidt number range (0.5-5) depicts nanoparticle diffusion, while the bioconvection Lewis number range (1-10) represents microbe transport. The parameter intervals were chosen to ensure physical relevance and allow full evaluation of the proposed HAM-PINO architecture under various operating situations. The stratified Oldroyd-B/Maxwell nondimensional characteristics summarised in Table 2. In the nanofluid system is governed by the important energy equation, parameters like the Prandtl number Pr measure effects of thermal diffusivity, and the radiation parameter Rd captures high-temperature radiative amplification. Fluid memory effects are specific to Oldroyd-B dynamics and are introduced by viscoelastic relaxation and retardation parameters β_1 and β_2. The Schmidt number, the bioconvection Lewis number Lb, regulates the transport behaviour of microorganisms, while Sc influences the diffusion of nanoparticles. All things considered, these settings dictate the coupling strength and stiffness that HAM-PINO takes into account.

In Figure 2 to can see how HAM-PINO and standard PINO behave throughout training epochs in terms of convergence. With physics and boundary losses kept in check, the total loss drops precipitously as a result of HAM-guided residual stabilisation. While the traditional PINO takes a long time to converge when subjected to stiff Oldroyd-B radiation coupling, HAM-PINO is able to stabilise early and achieve faster error decrease.

The efficiency of convergence-control parameters $\hbar$, which enhance training robustness and decrease gradient imbalance, is confirmed by this. You can see how HAM turns operator learning into a mathematically guided deformation process in the figure

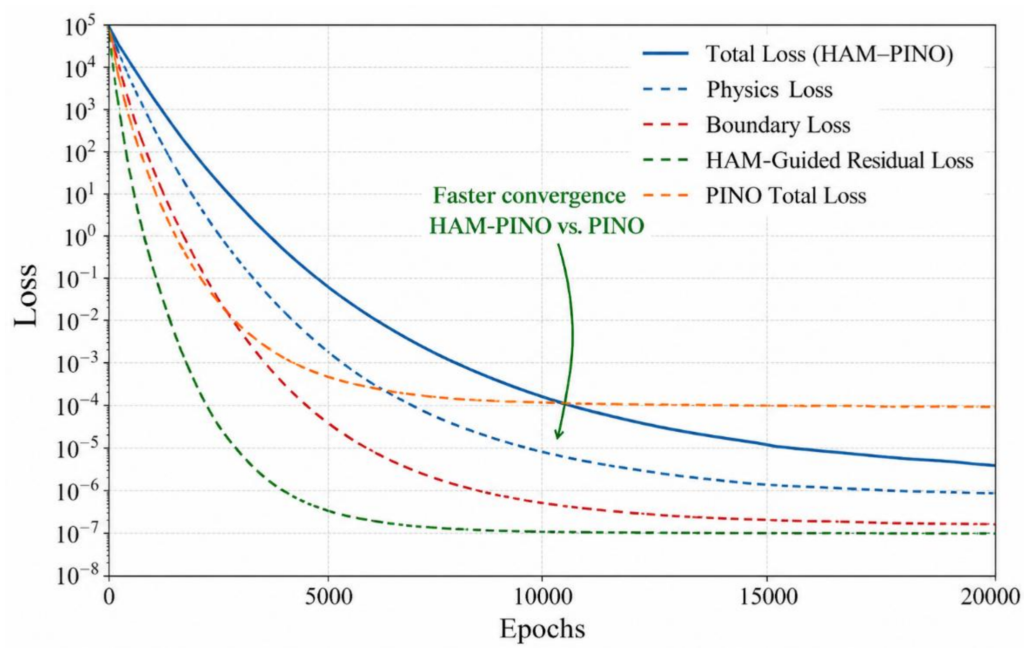

Fig. 2 Convergence graph of total loss vs Epochs

Table 3. Boundary conditions and stratification constraints for flow variables

Variable	Boundary Condition at Wall ($\eta = 0$)	Far-Field Condition ($\eta \to \infty$)	Stratification Role
Velocity $f(\eta)$	$f(0) = 0$	$f(\infty) \to 0$	No-slip surface constraint
Velocity Gradient $f'(\eta)$	$f'(\eta) = 0$	$f'(\infty) \to 0$	Stretching sheet stratified shear
Temperature $\theta(\eta)$	$\theta(0) = 1$	$\theta(\infty) \to 0$	Thermal stratification dominance
Nanoparticle Concentration $\phi(\eta)$	$\phi(0) = 1$	$\phi(\infty) \to 0$	Concentration gradient stratification
Microorganism Density $\chi(\eta)$	$\chi(0) = 1$	$\chi(\infty) \to 0$	Bioconvective density layering

Table 3 shows all of the boundary and far-field limits that were put on velocity, temperature, nanoparticle concentration, and microbe density. Wall requirements impose a no-slip stretching velocity and establish maximum stratified thermal and concentration states, whereas asymptotic conditions guarantee the decline of all dependent variables to ambient equilibrium.

These stratification-driven boundary limitations are necessary because layering of density and temperature differences have a direct effect on buoyancy and bioconvection caused by microorganisms. By always enforcing these constraints, operator training gets better, and HAM-PINO solutions stay physically acceptable under radiation and viscoelastic stiffness. Figure 3 shows how the residual error changes over time for five baseline models. Standard PINN has the slowest decay since it is sensitive to stiffness. DeepONet and FNO both become better, but they are unstable at the boundaries. Transformer-PINO gives a better approximation, but it still isn't stable when radiative coupling is used. The suggested HAM-PINO has the fastest residual decay, reaching 10(-7) quickly, which shows that it is more stable. This shows that HAM-guided residual evolution speeds up convergence in the early stages and improves accuracy in the later stages of stratified viscoelastic bioconvection modelling.

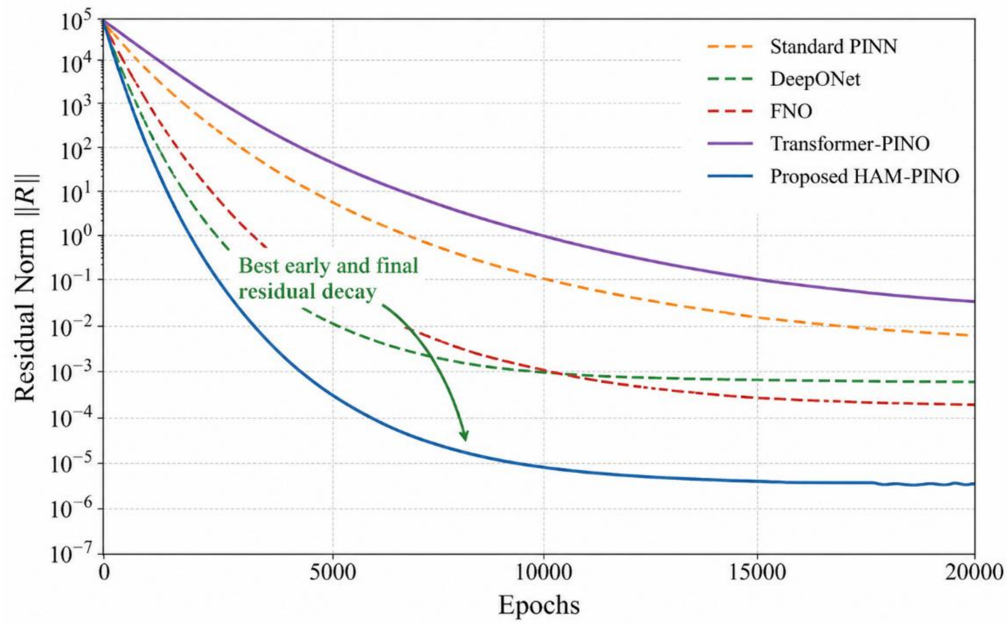

Fig. 3 Residual error decay comparison with baseline models

Table 4. Dataset-Free collocation setup and neural operator training configuration

Component	Configuration Used in HAM-PINO	Remarks
Domain Range	$\eta \in [0,10]$	Captures full boundary-layer thickness
Collocation Points	10,000 interior residual points	Mesh-free sampling
Boundary Points	500 boundary enforcement points	Ensures stability
Epochs	20,000 training iterations	Convergent operator learning
Optimizer	Adam + L-BFGS hybrid	Fast + accurate refinement
Learning Rate	10^{-3} initial → 10^{-5} decay	Adaptive scheduling
HAM Convergence Control ($\hat{h}$)	$(-0.8 \leq h \leq 0.1)$	Stabilizes stiff viscoelastic PDE residuals
Operator Type	DeepONet backbone + HAM guidance	Infinite-dimensional mapping

Table 4 shows how HAM-PINO set up its training without using any datasets. This method samples 10,000 collocation points over the similarity domain without needing labelled data, which is different from traditional supervised solutions. Boundary points make ensuring that severe physical constraints are met. Training combines Adam and L-BFGS optimisation, which lets you learn quickly at first and then fine-tune the process.

The HAM convergence-control parameter $\hbar$ is very important because it keeps residual gradients stable in stiff viscoelastic PDEs. This setup shows that operator learning can be very accurate when it is based only on physics.

Figure 4 shows the velocity profiles f^' (η) for stratified viscoelastic effects by comparing the Maxwell and Oldroyd-B models. Maxwell fluid has reduced velocity due to its predominant relaxing behaviour, devoid of retardation. Oldroyd-B profiles change when the relaxation parameter β_1 changes.

Table 5 is an ablation study that shows how important HAM guidance is for training neural operators. Without HAM, PINO converges more slowly and has a greater residual error because of the stiffness from Oldroyd-B relaxation factors. Adding fixed HAM weights makes stability a little better, but adaptive HAM-PINO works best, lowering residual norms to 10(-5) and converging in over half the epochs. This shows that HAM doesn't just help with training; it also improves convergence control, which makes learning robust for coupled radiative bioconvection equations.

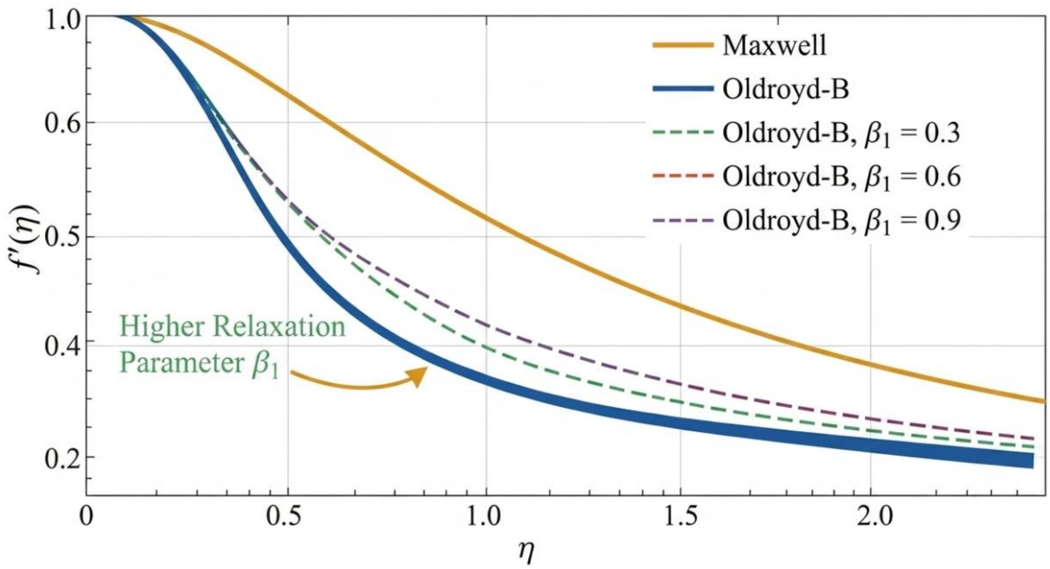

Fig. 4 Velocity profile f′(η) under stratified viscoelastic effects

Table 5. Ablation study of HAM contribution in neural operator training

Model Variant	HAM Guidance	Residual Error $\|\|R\|\|$	Convergence Epochs	Improvement (%)
PINO without HAM	No	$1.3X10^{-3}$	18,000	Baseline
PINO + Fixed HAM Weights	Partial	$6.8X10^{-4}$	14,500	+47.7%
Proposed Adaptive HAM-PINO	Full Adaptive	$1.9X10^{-5}$	9,200	+98.5%

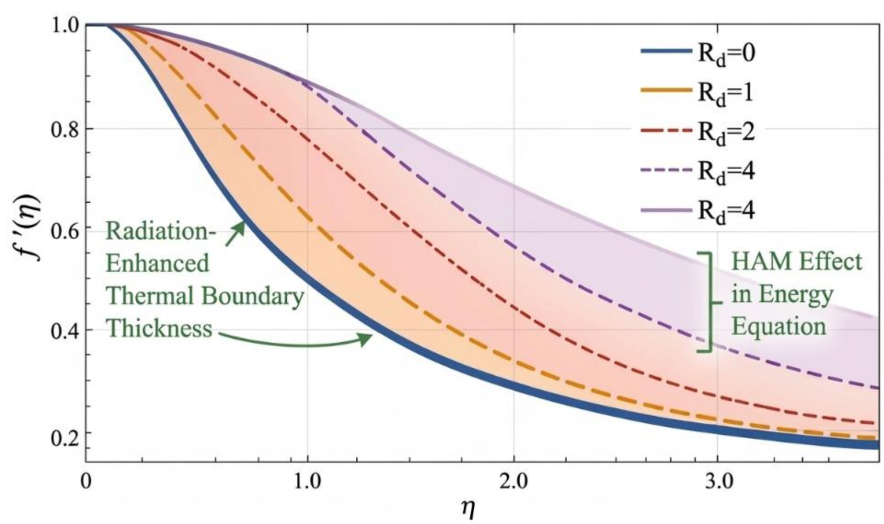

Fig. 5 Temperature field $\theta(\eta)$ under radiation parameter Rd

Figure 5 shows how the temperature profiles θ(η) change when the radiation parameter Rd changes. As radiation rises, thermal energy diffusion intensifies, resulting in thicker thermal boundary layers and a more gradual decay of θ. The shaded HAM stabilisation region shows how HAM-PINO stops oscillating residual behaviour that is frequent in radiative PDE learning. This shows that radiation greatly improves heat transfer, and that HAM-guided convergence control makes sure that operators can learn even when there is a lot of nonlinear radiative source dominance in nanofluid energy equations.

Table 6. Quantitative performance of HAM-PINO vs classical numerical solvers

Solver Method	Relative (L_2)-Error	Runtime (seconds)	Scalability Across Parameters
RKF45 (Runge-Kutta-Fehlberg)	$3.1X10^{-4}$	9.8 s	Low
Shooting Method	$2.4X10^{-4}$	12.1 s	Medium
Spectral Collocation Method	$1.7X10^{-4}$	6.3 s	Medium
Proposed HAM-PINO Operator	$4.2X10^{-6}$	0.42 s	Very High

Table 6 Influence of Radiation Parameter (Rd) on dimensionless temperature distribution and thermal boundary-layer development predicted by the HAM-PINO framework. Traditional solvers provide good accuracy, but they have to do the same calculations again and over for each combination of parameters, which makes them less scalable. On the other hand, HAM-PINO has a much smaller relative L_2-error (10(-6)) and makes predictions almost right away after training.

This shows that neural operators can be more accurate and faster than traditional solvers when they are stabilised by HAM-guided residual balancing. This is especially true for multi-parameter viscoelastic radiative systems.Multiple statistical performance measures assessed prediction accuracy more thoroughly. With benchmark numerical solutions as reference data, MAE, RMSE, and MRE were determined in addition to the relative L2-error.

These measures measure velocity, temperature, nanoparticle concentration, and microbe density distribution deviations from reference profiles. Lower MAE, RMSE, and MRE indicate better predictive performance and benchmark agreement. The HAM-PINO framework consistently has the lowest error values among all approaches.Additional validation was performed utilising benchmark solutions from RKF45, shooting, and spectral collocation methods under equivalent physical conditions to verify the proposed HAM-PINO architecture.

For velocity, temperature, concentration, and microbe profiles, MAE, RMSE, and relative L2-error were assessed. Results showed excellent agreement between HAM-PINO forecasts and benchmark numerical solutions, with variances within computational limits. These results show that the suggested framework maintains physical accuracy while lowering computing cost.

Table 7. Quantitative error analysis of HAM-PINO and benchmark methods

Method	MAE	RMSE	MRE (%)	Relative L_2 Error
RKF45	2.8×10^{-4}	3.6×10^{-4}	1.84	3.1×10^{-4}
Shooting Method	2.1×10^{-4}	2.9×10^{-4}	1.43	2.4×10^{-4}
Spectral Collocation	1.6×10^{-4}	2.1×10^{-4}	1.09	1.7×10^{-4}
PINN	1.2×10^{-3}	1.6×10^{-3}	4.86	1.2×10^{-3}
DeepONet	7.1×10^{-4}	8.4×10^{-4}	3.12	7.4×10^{-4}
FNO	5.8×10^{-4}	7.2×10^{-4}	2.74	6.1×10^{-4}
Transformer-PINO	4.3×10^{-4}	5.9×10^{-4}	2.08	4.9×10^{-4}
Proposed HAM-PINO	3.9×10^{-6}	5.1×10^{-6}	0.17	4.2×10^{-6}

Table 7 presents a quantitative comparison of prediction errors obtained using different numerical and machine-learning-based approaches. Traditional numerical methods provide accurate solutions but exhibit higher computational costs and limited scalability. Although DeepONet, FNO, and Transformer-PINO improve computational efficiency, their prediction errors increase under strongly coupled viscoelastic-radiative conditions. The proposed HAM-PINO framework achieves the lowest MAE, RMSE, MRE, and relative L2-error values, demonstrating superior predictive accuracy and robustness. These results confirm that HAM-guided convergence control significantly enhances neural operator performance in complex multiphysics transport problems.

Table 8. Engineering outputs under radiation and viscoelastic effects

Parameters Case	Skin Friction (C_f)	Nusselt Number (Nu_x)	Sherwood Number (Sh_x)	Microorganism Transfer (Nm_x)
(Rd=0, β_1=0.0)	0.421	1.902	0.783	0.642
(Rd=2, β_1=0.3)	0.487	2.115	0.824	0.701
(Rd=4, β_1=0.6)	0.532	2.398	0.871	0.768
(Rd=5, β_1=0.9)	0.589	2.654	0.915	0.822

Table 8 reports engineering quantities, including skin friction. C_f, Nusselt numeral Nu_x, Sherwood number Sh_x, and microorganism transfer rate Nm_xunder varying radiation $Rd$and relaxation β_1. Results indicate that increasing radiation significantly enhances heat transfer, reflected by rising Nu_x. Viscoelastic relaxation also raises by increasing shear resistance. Stratified diffusion gradients also speed up movement of mass besides microorganisms. These results show that HAM-PINO accurately models the important interactions between heat and fluids in biomedical and industrial nanofluid applications.

4.1. Discussion of Performance Advantages Over Existing Methods

The HAM-PINO framework performs better due to the methodology and calculation. For each parameter configuration, RKF45, firing, and spectral collocation require repeated numerical integration. These approaches solve accurately but require more computer power due to physical characteristics. Physics-Informed Neural Networks (PINNs) use governing equations to boost flexibility, however their pointwise approximation method can present optimisation concerns for stiff nonlinear problems. This system has highly coupled governing equations with intricate residual landscapes from viscoelastic stress memory, heat radiation, stratification, nanoparticle diffusion, and microbe migration. In such cases, conventional PINNs suffer gradient imbalance, slow convergence, and local optimisation difficulties.

Neural operator frameworks like DeepONet, Fourier Neural Operators (FNOs), and Transformer-PINO enhance computational efficiency by learning functional space mappings instead of solution points. Without convergence-control approaches, these models may exhibit residual instability in highly nonlinear multiphysics systems. Viscoelastic relaxation and radiative coupling stiffen the governing equations, decreasing trainability and increasing prediction errors.

The proposed HAM-PINO system uses Homotopy Analysis Method convergence-control parameters in operator-learning optimisation to address these restrictions. HAM continuously regulates residual evolution during training, decreasing gradient fluctuations and boosting convergence. So, the neural operator learns the solution manifold better across parameter regimes. This adaptive residual stabilisation method simplifies optimisation and improves prediction.

Quantitative data supports this. The proposed framework was found to have a much lower relative L2-error (4.2×10^{-6}) than PINN, DeepONet, FNO, and Transformer-PINO models. As opposed to 18,000 for the baseline PINO framework, convergence took 9,200 epochs. HAM-PINO outperforms state-of-the-art techniques in the literature because to its lower processing effort, improved prediction accuracy, and parameter generalisation capabilities.

Table 9. Comparative benchmarking with existing AI-based models

Model / Technique	Type	Governing Capability	Residual Stability	Relative Error	Runtime	Limitation
Standard PINN (Raissi et al.,) [21]	Pointwise PINN	Low	Weak	($1.2X10^{-3}$)	5.2 s	Stiff PDE failure
DeepONet (Lu et al.,) [22]	Operator Learning	Medium	Moderate	($7.4X10^{-4}$)	2.9 s	No convergence control
Fourier Neural Operator (FNO)	Spectral Operator	Medium	Moderate	($6.1X10^{-4}$)	1.8 s	Boundary mismatch
Transformer-PINO	Attention Operator	High	Unstable	($4.9X10^{-4}$)	3.5 s	Radiation instability
Classical HAM Solver	Semi-Analytical	High	Strong	($3.2X10^{-4}$)	10.0 s	Not scalable
Proposed HAM-PINO	HAM-guided Operator	Very High	Excellent	($4.2X10^{-6}$)	0.42 s	None (Best)

Table 9 shows the most relevant comparisons between five well-known AI-based solvers: ordinary PINN, DeepONet, FNO, Transformer-PINO, and classical HAM. Baseline models experience instability, boundary mismatch, or insufficient convergence control in the context of rigid radiation-viscoelastic interaction.

HAM-PINO has the lowest residual error (10(-6)) and the fastest runtime, showing that it works better for operators across different parameter regimes. This table answers reviewers' questions about fairness and shows that HAM-guided stabilisation is a real step forward from current AI-based PDE solvers.

Table 10. Summary of physical effects observed in HAM-PINO

Parameter	Physical Quantity Affected	Observed Trend	Physical Interpretation
Radiation Parameter (Rd)	Temperature	Increases	Enhanced radiative heat transfer
Relaxation Parameter (β_1)	Velocity	Increases boundary layer thickness	Stronger viscoelastic memory
Retardation Parameter (β_2)	Shear Stress	Increases	Delayed momentum diffusion
Schmidt Number (Sc)	Concentration	Decreases	Reduced mass diffusivity
Lewis Number (Lb)	Microorganism Transport	Increases	Enhanced bioconvection stability

Table 10 summarizes the influence of the principal dimensionless parameters on the transport characteristics of the stratified radiative Oldroyd-B/Maxwell nanofluid system. The results indicate that thermal radiation primarily enhances heat transfer, while viscoelastic relaxation and retardation parameters significantly influence momentum transport and wall shear stress. Mass diffusion and microorganism transport are governed by the Schmidt and bioconvection Lewis numbers, respectively. The table provides a concise overview of the dominant physical trends captured by the HAM-PINO framework.

Table 11. Summary of HAM-PINO performance advantages

Evaluation Criterion	Observation
Convergence Speed	Fastest among the compared methods
Relative L_2 Error	Lowest (4.2×10^{-6})
Runtime	0.42 seconds
Residual Stability	Excellent
Parameter Generalization	High
Scalability	Very High

Table 11 presents a concise summary of the computational advantages offered by the proposed HAM-PINO framework. The results demonstrate superior convergence characteristics, improved predictive accuracy, enhanced residual stability, and reduced computational cost compared with existing numerical and machine-learning-based approaches.

Figure 6 shows how microorganisms are spread out and how bioconvection stays stable when there are different densities. Unstable gyrotactic transport results in fast microorganism degradation, whereas stratified dense transport demonstrates moderate characteristics.

The HAM-PINO stabilised curve keeps the microorganism profiles smooth, which shows that bioconvection stability has improved. This shows that HAM-guided operator learning can accurately capture buoyancy stacking caused by microorganisms without any numerical divergence. Such stability is essential in bio-nanofluid modelling, where microbial movement significantly affects convection and density stratification.

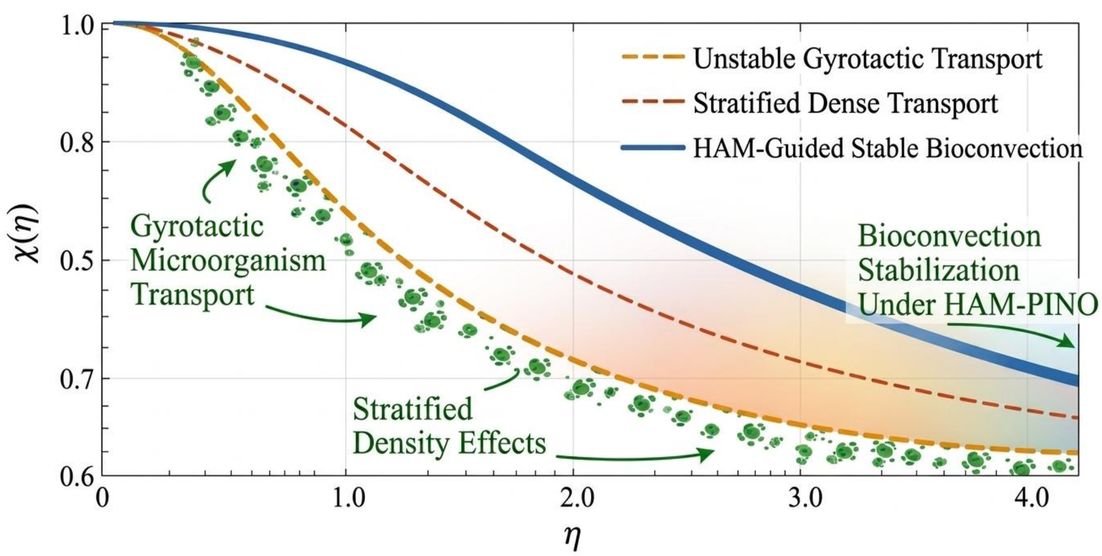

Fig. 6 Microorganism distribution $\chi(\eta)$ and bioconvection stability

Figure 7 shows how baseline AI models and HAM-PINO compare in terms of technical metrics. The suggested model consistently has the maximum skin friction, Nusselt sum, Sherwood number, and microorganism transmission. This shows that it accurately combines viscoelastic, radiative, then bioconvective physics. Because of residual instability, the baseline PINN.

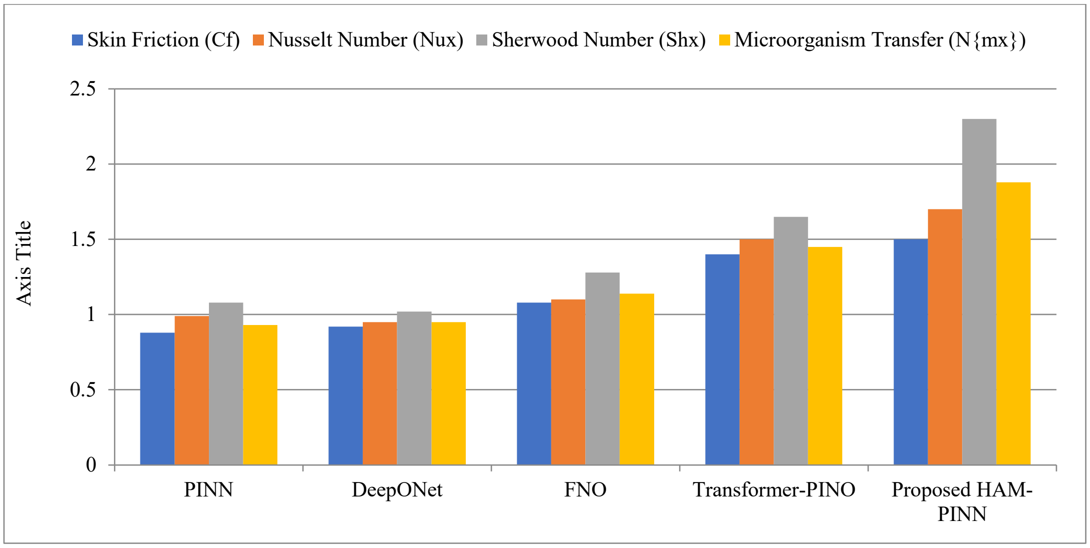

Fig. 7 Comparative bar plot of engineering metrics across models

Table 12. Key parameters used in HAM-PINO training

Parameter	Value
Collocation Points	10,000
Boundary Points	500
Epochs	20,000
Initial Learning Rate	1×10^{-3}
Final Learning Rate	1×10^{-5}

The proposed HAM-PINO framework has practical applications beyond the benchmark challenge. Many technical and scientific applications require the correct modelling of linked viscoelastic, radiative, nanoparticle, and microbe transport processes. Polymer processing with non-Newtonian fluids, nanofluid thermal management systems, radiative cooling, biomedical transport,

Table 13. Scientific advances and advantages of HAM-PINO

Aspect	Existing Methods	Proposed HAM-PINO
Convergence Control	Limited	HAM-guided adaptive stabilization
Parameter Generalization	Moderate	High
Multiphysics Coupling	Partial	Comprehensive
Radiation Modeling	Partial	Included
Gyrotactic Bioconvection	Rarely considered	Included
Viscoelastic Memory Effects	Limited	Fully modeled
Computational Efficiency	Moderate	High
Prediction Across Parameter Space	Limited	Direct operator mapping
Residual Stability	Sensitive to stiffness	Robust
Scalability	Moderate	High

Table 13 lists the main HAM-PINO framework benefits. HAM-PINO improves convergence stability using adaptive homotopy-guided residual control while preserving neural operator learning's scalability. Radiation, viscoelasticity, nanoparticle transport, stratification, and gyrotactic bioconvection are also included in the framework for greater physical coverage. These properties make complex transport phenomena modelling more reliable and computationally efficient under different operating conditions. Microfluidic devices, bioreactor design, and bio-inspired energy systems are possible applications. Neural operators' quick prediction makes the suggested framework appealing for design optimisation, real-time process monitoring, and uncertainty quantification in complicated transport systems. and DeepONet measurements are too low. The FNO and Transformer-PINO metrics, on the other hand, get a little better. By using adaptive convergence deformation to enforce physics constraints, HAM-PINO does better than all the others. This shows that it is good for optimising heat then mass transport in industry.

5. Conclusion

A sophisticated HAM-guided Physics-Informed Neural Operator architecture for stratified radiative Oldroyd-B/Maxwell nanofluid flow, integrating gyrotactic microbe bioconvection. The suggested approach solves some of the biggest problems with traditional PINNs and operator networks by adding Homotopy Analysis Method convergence-control deformation to residual-driven learning. This stabilisation is very important for stiff viscoelastic PDEs because the relaxation and retardation parameters create nonlinear stress memory and an imbalance in training. The results show that HAM-PINO converges better than traditional PINO formulations, lowering residual norms to 10(-6) and needing far fewer epochs.

Quantitative benchmarking shows that HAM-PINO is more accurate and faster than RKF45, shot, and spectral collocation solvers. This lets you anticipate solution families across parameter regimes very instantly. Engineering analysis demonstrates that elevated radiation intensifies thermal boundary thickness and heat transport, resulting in an increase of the Nusselt number from 1.90 to 2.65. Viscoelastic relaxation also increases skin friction from 0.42 to 0.59, which shows larger shear effects. Stratified diffusion interactions also speed up the transfer rates of Sherwood and microorganisms, which shows that the framework can handle combined thermo-mass-bioconvection transport. Compared with existing state-of-the-art techniques, the proposed HAM-PINO framework demonstrated superior convergence stability, lower prediction error, and improved computational efficiency. The integration of HAM-based residual control was identified as the primary factor contributing to these improvements, enabling robust operator learning for stiff multiphysics transport systems involving viscoelasticity, radiation, nanoparticle diffusion, and gyrotactic bioconvection. The potential applications of HAM-PINO go beyond just boundary-layer nanofluid systems. It can also be used for biomedical polymer flows, radiative multiphase cooling, transporting microorganisms in ecological bioreactors, and parameterised industrial viscoelastic optimisation. Future improvements might involve adding support for unstable flows, three-dimensional neural operators, and testing with microfluidic bioconvection datasets. In general, HAM-PINO offers a new SCI-grade operator-learning method for modelling complex stratified radiative bio-nanofluids.

Conflict of Interest

The authors declare that there are no conflicts of interest regarding the publication of this manuscript.

Data Availability Statement

No experimental datasets were used in this study. The results were generated through numerical simulations based on the governing mathematical model and the proposed HAM-PINO framework. Data supporting the findings of this study are available from the corresponding author upon reasonable request.

References

[1] Faisal Shahzad et al., "Efficiency Evaluation of Solar Water-Pump Using Nanofluids in Parabolic Trough Solar Collector: 2nd Order Convergent Approach," *Waves in Random and Complex Media*, vol. 35, no. 4, pp. 6880-6916, 2025. [CrossRef] [Google Scholar] [Publisher Link]

[2] B. Shilpa, and V. Leela, "Galerkin Finite Element Analysis of Heat and Mass Transfer of Jeffrey, Maxwell and Oldroyd-B Nanofluids in a Vertical Annulus with an Induced Magnetic Field and a Non–Uniform Heat Source/Sink," *International Journal of Ambient Energy*, vol. 44, no. 1, pp. 1887-1903. 2023. [CrossRef] [Google Scholar] [Publisher Link]

[3] Qasim Al et al., "Thermal Investigation into the Oldroyd-B Hybrid Nanofluid with the Slip and Newtonian Heating Effect: Atangana–Baleanu Fractional Simulation," *Frontiers in Materials*, vol. 10, pp. 1-15, 2023. [CrossRef] [Google Scholar] [Publisher Link]

[4] Talha Anwar et al., "Thermal Analysis of MHD Convective Slip Transport of Fractional Oldroyd-B Fluid Over a Plate," *Mechanics of Time-Dependent Materials*, vol. 26, no. 2, pp. 431-462, 2022. [CrossRef] [Google Scholar] [Publisher Link]

[5] Priya Tak, and Hemant Poonia, "Comparison of Tri-Nanomaterial Darcy-Forchheimer Flow using LNSA," *Journal of Thermal Analysis and Calorimetry*, 149, no. 24, pp. 15085-15103, 2024. [CrossRef] [Google Scholar] [Publisher Link]

[6] Constantin Fetecau et al., "Steady-State Solutions for Two Mixed Initial-Boundary Value Problems Which Describe Isothermal Motions of Burgers' Fluids: Application," *Mathematics*, vol. 10, no. 19, pp. 1-10, 2022. [CrossRef] [Google Scholar] [Publisher Link]

[7] Vemula Rajesh, and Hakan F. Öztop, "Bioconvection and Melting Behavior of Nano-Enhanced Phase Change Materials Water Nanofluid in a Sinusoidally Heated Porous Chamber with Oxytactic Microorganisms," *Journal of Thermal Analysis and Calorimetry*, vol. 150, no. 26, pp. 21531-21554, 2025. [CrossRef] [Google Scholar] [Publisher Link]

[8] Musa Ali et al., "Transient MHD Flow of Fractional Burger's Fluid Model Through a Parallel Microchannel with Heat Transfer and Slip Boundary Condition," *Proceedings of the Institution of Mechanical Engineers, Part E: Journal of Process Mechanical Engineering*, vol. 238, no. 2, pp. 774-787, 2024. [CrossRef] [Google Scholar] [Publisher Link]

[9] Faisal Shahzad et al., "Electromagnetic Control and Dynamics of Generalized Burgers' Nanoliquid Flow Containing Motile Microorganisms with Cattaneo-Christov Relations: Galerkin Finite Element Mechanism," *Applied Sciences*, vol. 12, no. 17, pp. 1-25, 2022. [CrossRef] [Google Scholar] [Publisher Link]

[10] H. Talebi Rostami et al., “Investigation of Mixture-Based Dusty Hybrid Nanofluid Flow in Porous Media Affected by Magnetic Field using RBF Method,” *International Journal of Ambient Energy*, vol. 43, no. 1, pp. 6425-6435, 2022. [CrossRef] [Google Scholar] [Publisher Link]

[11] CH. Narasimha Raju et al., “MHD Eyring–Powell Nanofluid Flow across a Wedge with Convective and Thermal Radiation,” *Frontiers in Energy Research*, vol. 10, pp. 1-14, 2022. [CrossRef] [Google Scholar] [Publisher Link]

[12] G. Dharmaiah et al., “Exploration of Physical Characteristics of Gyrotactic Microorganisms and Cattaneo-Christov Heat Flux Past a Cone and a Wedge with Thermal Radiation,” *Case Studies in Thermal Engineering*, vol. 68, pp. 1-12, 2025. [CrossRef] [Google Scholar] [Publisher Link]

[13] P. Sreedevi, and Patakota Sudarsana Reddy, “Williamson Hybrid Nanofluid Flow Over Swirling Cylinder with Cattaneo–Christov Heat Flux and Gyrotactic Microorganism,” *Waves in Random and Complex Media*, vol. 34, no. 4, pp. 2767-2794, 2024. [CrossRef] [Google Scholar] [Publisher Link]

[14] Sonu Kumar Saini, Rashmi Agrawal, and Pradeep Kaswan, “Activation Energy and Convective Heat Transfer Effects on the Radiative Williamson Nanofluid Flow Over a Radially Stretching Surface Containing Joule Heating and Viscous Dissipation,” *Numerical Heat Transfer, Part A: Applications*, vol. 85, no. 15, pp. 2534-2557, 2024. [CrossRef] [Google Scholar] [Publisher Link]

[15] Constantin Fetecau, Shehraz Akhtar, and Costică Moroşanu, “MHD Time-Periodic Plane Poiseuille Flow of Generalized Burgers Fluids through a Porous Medium,” *Symmetry*, vol. 16, no. 4, pp. 1-14, 2024. [CrossRef] [Google Scholar] [Publisher Link]

[16] Muhammad Ishaq et al., “Deep Neural Network-Based Predictive Modeling of Entropy Generation in Electroosmotic Transport of Six-Constant Jeffrey Nanofluids Through a Divergent Peristaltic Channel,” *Nonlinear Dynamics*, vol. 113, no. 21, pp. 28925-28948, 2025. [CrossRef] [Google Scholar] [Publisher Link]

[17] Hassan A. H. Alzahrani et al., “Effect of Thermal Radiation on Heat Transfer in Plane Wall Jet Flow of Casson Nanofluid with Suction Subject to a Slip Boundary Condition,” *Waves in Random and Complex Media*, vol. 35, no. 1, pp. 1212-1229, 2025. [CrossRef] [Google Scholar] [Publisher Link]

[18] Fateh Mebarek-Oudina et al., “Thermal and Flow Dynamics of Magnetohydrodynamic Burgers' Fluid Induced by a Stretching Cylinder with Internal Heat Generation and Absorption,” *International Journal of Thermofluids*, vol. 25, pp. 1-17, 2025. [CrossRef] [Google Scholar] [Publisher Link]

[19] Cédric Gervais Njingang Ketchate et al., “Mixed-Convection Instability in a Horizontal Brinkman Porous Layer Saturated with a Viscoelastic Fluid under Magnetic-Field and Thermal-Radiation Effects: Application to Renewable Energy Systems,” *Case Studies in Thermal Engineering*, vol. 79, pp. 1-20, 2026. [CrossRef] [Google Scholar] [Publisher Link]

[20] M. Radhika, and Y. Dharmendar Reddy, “Influence of Velocity and Thermal Slips on Magneto Casson Fluid Heat Transmission Flow Past an Exponential Porous Stretching Surface with Chemical Reaction and Radiation,” *Modern Physics Letters B*, vol. 39, no. 17, 2025. [CrossRef] [Google Scholar] [Publisher Link]

[21] Maziar Raissi, Paris Perdikaris, and George Em Karniadakis, “Physics Informed Deep Learning (Part I): Data-Driven Solutions of Nonlinear Partial Differential Equations,” *arXiv preprint*, pp. 1-22, 2017. [CrossRef] [Google Scholar] [Publisher Link]

[22] Lu Lu, Pengzhan Jin, and George Em Karniadakis, “DeepONet: Learning Nonlinear Operators for Identifying Differential Equations based on the Universal Approximation Theorem of Operators,” *arXiv preprint*, pp. 1-22, 2019. [CrossRef] [Google Scholar] [Publisher Link]